AMERICAN SOCIETY FOR MICROBIOLOGY | Journal of Virology®

PATHOGENESIS AND IMMUNITY

Intrinsic Innate Immune Responses Control Viral Growth and Protect against Neuronal Death in an *Ex Vivo* Model of West Nile Virus-Induced Central Nervous System Disease

Penny Clarke,[a] J. Smith Leser,[a] Kenneth L. Tyler[a,b,c,d,e]

[a]Department of Neurology, University of Colorado, Anschutz Medical Campus, Aurora, Colorado, USA
[b]Department of Medicine, University of Colorado, Anschutz Medical Campus, Aurora, Colorado, USA
[c]Department of Immunology and Microbiology, University of Colorado, Anschutz Medical Campus, Aurora, Colorado, USA
[d]Department of Infectious Disease, University of Colorado, Anschutz Medical Campus, Aurora, Colorado, USA
[e]Department of Veterans Affairs, Aurora, Colorado, USA

ABSTRACT Recruitment of immune cells from the periphery is critical for controlling West Nile virus (WNV) growth in the central nervous system (CNS) and preventing subsequent WNV-induced CNS disease. Neuroinflammatory responses, including the release of proinflammatory cytokines and chemokines by CNS cells, influence the entry and function of peripheral immune cells that infiltrate the CNS. However, these same cytokines and chemokines contribute to tissue damage in other models of CNS injury. Rosiglitazone is a peroxisome proliferator-activated receptor gamma (PPARγ) agonist that inhibits neuroinflammation. We used rosiglitazone in WNV-infected *ex vivo* brain slice cultures (BSC) to investigate the role of neuroinflammation within the CNS in the absence of peripheral immune cells. Rosiglitazone treatment inhibited WNV-induced expression of proinflammatory chemokines and cytokines, interferon beta (IFN-β), and IFN-stimulated genes (ISG) and also decreased WNV-induced activation of microglia. These decreased neuroinflammatory responses were associated with activation of astrocytes, robust viral growth, increased activation of caspase 3, and increased neuronal loss. Rosiglitazone had a similar effect on *in vivo* WNV infection, causing increased viral growth, tissue damage, and disease severity in infected mice, even though the number of infiltrating peripheral immune cells was higher in rosiglitazone-treated, WNV-infected mice than in untreated, infected controls. These results indicate that local neuroinflammatory responses are capable of controlling viral growth within the CNS and limiting neuronal loss and may function to keep the virus in check prior to the infiltration of peripheral immune cells, limiting both virus- and immune-mediated neuronal damage.

IMPORTANCE West Nile virus is the most common cause of epidemic encephalitis in the United States and can result in debilitating CNS disease. There are no effective vaccines or treatments for WNV-induced CNS disease in humans. The peripheral immune response is critical for protection against WNV CNS infections. We now demonstrate that intrinsic immune responses also control viral growth and limit neuronal loss. These findings have important implications for developing new therapies for WNV-induced CNS disease.

KEYWORDS innate immune response, West Nile virus, CNS disease, neuroinflammation, rosiglitazone

West Nile virus (WNV) is a neurotropic, single-stranded RNA virus in the genus *Flavivirus*. The vast majority of WNV infections are either asymptomatic or result in an acute febrile illness. However, a small percentage (less than 1%) of human WNV infections cause neurological disease, including meningitis, encephalitis, or acute flaccid paralysis (1, 2). Since its

Citation Clarke P, Leser JS, Tyler KL. 2021. Intrinsic innate immune responses control viral growth and protect against neuronal death in an *ex vivo* model of West Nile virus-induced central nervous system disease. J Virol 95: e00835-21. https://doi.org/10.1128/JVI.00835-21.

Editor Mark T. Heise, University of North Carolina at Chapel Hill

Address correspondence to Penny Clarke, penny.clarke@cuanschutz.edu.

Received 18 May 2021
Accepted 19 June 2021
Accepted manuscript posted online 30 June 2021
Published 25 August 2021

introduction to New York, United States, in 1999, there have been more than 25,000 cases of WNV-induced neuroinvasive disease, and WNV is currently the most common cause of epidemic viral encephalitis in the United States (https://www.cdc.gov/westnile). Mortality in patients with WNV-induced neuroinvasive disease is around 10% (https://www.cdc.gov/westnile), and 50% of surviving patients have long-lasting neurological sequelae (reviewed in reference 3). There are no available human vaccines or antivirals targeting WNV, and a better understanding of the pathogenesis of WNV-induced CNS disease is needed to develop effective treatment strategies.

WNV infects neurons within the CNS. Subsequent caspase 3-dependent apoptotic cell death contributes to WNV-induced CNS disease (4, 5). The neuroinflammatory response to WNV infection, comprising robust microglial activation (4, 6–11) and astrogliosis (4, 11–13), immune cell infiltration from the periphery (14–21), and significant expression of proinflammatory cytokines/chemokines (4, 22), also plays a role in WNV-induced CNS disease. Neuroinflammatory responses can be protective. For example, infection of mouse CNS tissue with WNV results in classical (M1) activation of microglia, which limits viral growth in the CNS and protects against virus-induced CNS disease (23, 24). Microglial activation is associated with upregulation of proinflammatory cytokines, such as tumor necrosis factor alpha (TNF-α) and interleukin-6 (IL-6), and chemokines, such as C-C motif chemokine ligand 2 (CCL2), C-X-C motif chemokine ligand 10 (CXCL10), and CCL5 (4, 22). These proinflammatory mediators promote infiltration of peripheral immune cells into the CNS following WNV infection and regulate their function, controlling virus growth and facilitating viral clearance (14, 17, 19, 25, 26). Astrocytes and neurons also release cytokines and chemokines following infection and may be the primary producers of CCL5 and CXCL10, respectively, following WNV CNS infection (14, 17). Another subset of cytokines that are upregulated in the CNS following WNV infection and are critical for protection against WNV-induced CNS disease are type 1 interferons (IFNs), including IFN-α and IFN-β. Type 1 IFNs stimulate the expression of hundreds of IFN-stimulated genes (ISGs) with antiviral functions that act to curb the growth of many viruses in the CNS (27, 28). Although cytokines and chemokines play an important role in preventing viral growth in the CNS and clearing the infection, these same molecules are known to contribute to multiple pathogenic CNS states (reviewed in reference 29). The extent to which chemokine/cytokines are released as part of the neuroinflammatory response to WNV infection contribute to WNV-induced CNS disease is unclear. West Nile virus-induced memory T cells have been shown to promote microglia-mediated synaptic elimination in mice, leading to learning and memory deficits and may contribute to long-term neurologic deficits seen in recovering patients (30). In addition, TNF-α signaling has been shown to contribute to neuronal death following WNV infection may contribute to chronic inflammation and long-term morbidity in some WNV survivors (31, 32).

West Nile virus infection of *ex vivo* brain (BSC) and spinal cord (SCSC) cultures provide models of WNV infection of the CNS that replicate critical hallmarks of WNV infection *in vivo*, including high levels of neuronal infection and caspase-mediated apoptotic death (4, 11, 33). We previously used these cultures to demonstrate that CNS parenchymal cells (including neurons, microglia, and astrocytes) are capable of mounting intrinsic immune responses to WNV, such as robust microglial activation and astrogliosis, and significant expression of proinflammatory cytokines/chemokines, in the absence of potentially confounding contributions from peripheral immune cells (4, 11, 33). In this report, we used the peroxisome proliferator-activated receptor gamma (PPARγ) agonist rosiglitazone to investigate the role of neuroinflammation during WNV infection of BSC. Several studies have reported that PPARγ agonists inhibit the activity of NF-κB, leading to decreased expression of proinflammatory genes and polarization of microglia to an anti-inflammatory (M2) phenotype (34–39). The anti-inflammatory effects of PPARγ are protective in several models of CNS injury and disease (39–49). In contrast to these studies, in this report, we show that rosiglitazone treatment was not protective in WNV-infected BSC. Rosiglitazone treatment resulted in exacerbated neuronal death and increased viral titers

that were associated with decreased expression of proinflammatory and antiviral chemokines/cytokines and decreased microglial activation. *In vivo* results demonstrated that rosiglitazone treatment similarly increased the severity of WNV-induced CNS disease in mice. Our results indicate that local neuroinflammatory responses protect against WNV-induced CNS disease.

RESULTS

Rosiglitazone inhibits WNV-induced expression of proinflammatory and antiviral cytokines/chemokines in BSC. We have previously shown that WNV induces the expression of proinflammatory genes in the brains of infected mice (4, 22) and in *ex vivo* brain (BSC) and spinal cord (SCSC) slice cultures (4, 11, 33). In order to investigate the role of proinflammatory gene expression within the CNS, we infected BSC with 10^5 PFU per slice in the presence/absence of 20 μM rosiglitazone (50). Concentrations of rosiglitazone higher than 20 μM resulted in decreased viability of uninfected BSC (data not shown). Five days following infection, cultures were harvested, and RNA was prepared. As expected from previous work (11, 33), quantitative reverse transcription PCR (RT-qPCR) analysis revealed that WNV-infection of BSC resulted in significantly increased expression of the proinflammatory chemokines/cytokines CCL5, CXCL10, CCL2, IL-6, and TNF-α compared to mock-infected slices (Fig. 1A). WNV-induced increases in expression of proinflammatory chemokines/cytokines were inhibited in rosiglitazone-treated slices compared to vehicle-treated controls (Fig. 1A). WNV-induced increases in the expression of proinflammatory chemokines/cytokines were not inhibited in slices treated with both rosiglitazone and the PPARγ inhibitor GW9662 (20 μM; Fig. 1A). These results indicate that rosiglitazone inhibits WNV-induced expression of proinflammatory genes at the RNA level and that this inhibition is due to its function as a PPARγ agonist. Enzyme-linked immunosorbent assays (ELISAs) confirmed the upregulation of selected chemokines/cytokines following WNV infection of BSC. The expression of CCL5, IL-6, and TNF-α was significantly upregulated. CCL2 was also upregulated, but the increase did not quite reach significance. ELISA also confirmed that rosiglitazone treatment inhibited this upregulation (Fig. 1B). Since prior studies have indicated that rosiglitazone promotes an anti-inflammatory (M2) environment, we also investigated the expression of IL-10 and IL-4 in WNV-infected BSC. Treatment of BSC with rosiglitazone resulted in increased expression of IL-10 and IL-4 in BSC following WNV infection compared to untreated, infected controls, suggesting that rosiglitazone promotes an anti-inflammatory environment in WNV-infected BSC (Fig. 1C). Rosiglitazone treatment also inhibited the WNV-induced expression of IFN-β and the ISG IFN regulatory factor 1 (IRF1), MX dynamin-like GTPase 1 (MX1), and IFN-induced protein with tetratricopeptide repeats 1 (IFIT1) (Fig. 1D). Taken together, these results demonstrate that rosiglitazone treatment of WNV-infected BSC results in broad inhibition of WNV-induced neuroinflammatory responses, including downregulation of proinflammatory chemokines and cytokines, downregulation of IFN-β and ISG, and upregulation of anti-inflammatory genes.

Rosiglitazone inhibits microglial activation and leads to increased viral titer in WNV-infected BSC. The neuroinflammatory response to WNV includes the activation of microglia and astrocytes. RT-qPCR analysis demonstrated that WNV infection of BSC resulted in increased expression of the microglial marker, ionized calcium binding adaptor molecule 1 (Iba1), compared to mock-infected BSC and that this was decreased in the presence of rosiglitazone (Fig. 2A). In contrast, WNV-induced expression of the astrocyte marker glial fibrillary acidic protein (GFAP) was upregulated at the RNA level in rosiglitazone-treated, WNV-infected BSC compared to untreated, infected controls (Fig. 2A). Decreased expression of Iba1 in rosiglitazone-treated, WNV-infected slices was associated with increased viral load as determined by RT-qPCR (Fig. 2B). Visualization of WNV-infected slices by immunohistochemistry also demonstrated decreased Iba1 and increased GFAP staining in rosiglitazone treated, WNV-infected BSC compared to untreated, infected controls (Fig. 2C). Counterstaining of WNV-infected slices with WNV antibody revealed that levels of WNV antigen were increased in WNV-infected, rosiglitazone-treated slices compared to untreated, WNV-infected controls (Fig. 2C). Costaining of cells with Iba1 and WNV

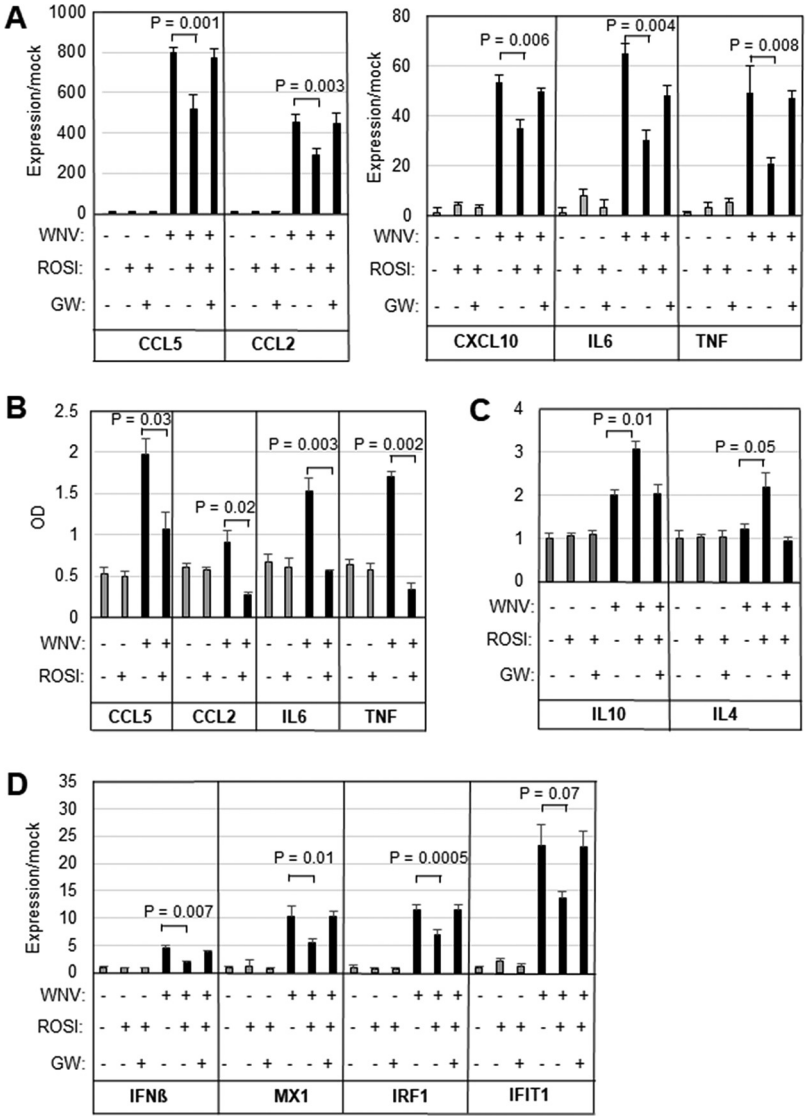

FIG 1 Rosiglitazone inhibits WNV-induced expression of proinflammatory and antiviral cytokines/chemokines in *ex vivo* BSC. BSC were infected with WNV (10^5 PFU per slice) in the presence/absence of 20 μM rosiglitazone (ROSI) (A to D). Five days following infection, cultures were harvested, and RNA or protein lysates were prepared. WNV-induced expression of proinflammatory cytokines (A and B), anti-inflammatory cytokines (C), and IFN-related genes (D) is shown. GW9662 (GW; 20 μM), an inhibitor of PPARγ signaling, reversed the effect of rosiglitazone. The graphs show the average increased expression over mock (A, C, and D) or average optical density reading ($n = 3$). Error bars indicate the standard error of the mean. Statistical significance was determined using 2-sample, 2-tailed *t* tests (GraphPad).

antigen was not seen, substantiating previous studies that have suggested that microglia are not infected by WNV in *ex vivo* cultures (11). In contrast, some GFAP-positive cells did appear to contain WNV antigen, indicating that WNV can infect astrocytes (Fig. 2C).

Rosiglitazone increases apoptotic neuronal loss in WNV-infected BSC. Caspase 3-mediated neuronal death is a hallmark of WNV-induced tissue injury and CNS disease (4, 5). We investigated caspase 3 activity and neuronal death in WNV-infected BSC following rosiglitazone treatment. BSC were infected with WNV (10^5 PFU per slice). Seven days postinfection, slices were harvested for protein lysate or were fixed for immunohistochemistry (IHC) analysis. *In vitro* fluorogenic caspase 3 activity assays revealed that rosiglitazone treatment increased WNV-induced activation of caspase 3 in infected BSC compared to untreated controls (Fig. 3A). Immunohistochemistry also revealed increased neuronal death in WNV-infected BSC in the presence of rosiglitazone as

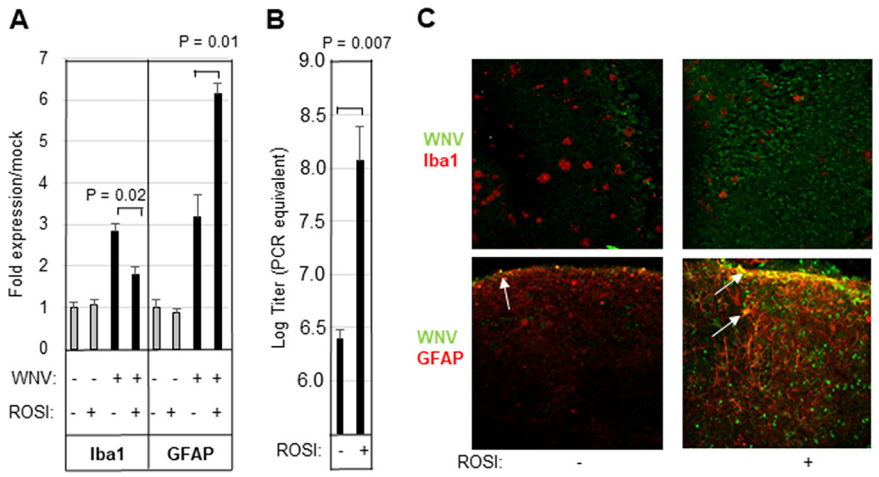

FIG 2 Rosiglitazone inhibits microglial activation and leads to increased viral titer in WNV-infected BSC. BSC were infected with WNV (10^5 PFU per slice) in the presence/absence of 20 μM rosiglitazone (ROSI). (A to C) Five days following infection, cultures were harvested, and RNA was prepared. WNV-induced expression of microglial (Iba1) and astrocyte (GFAP) markers (A, average increased expression over mock), as well as viral titer (B, average titer) is shown. Error bars indicate the standard error of the mean ($n = 3$). Statistical significance was determined using 2-sample, 2-tailed *t* tests (GraphPad). (C) WNV-infected slices were also examined by immunohistochemistry. The images show decreased Iba1 staining (red staining in upper images) in rosiglitazone-treated, WNV-infected slices compared to untreated, infected controls. In contrast, rosiglitazone treatment of WNV-infected BSC resulted in increased GFAP expression (red staining in lower images) compared to untreated, infected controls. Counterstaining of slices with WNV antibody (green staining) revealed increased viral antigen in rosiglitazone slices compared to untreated, WNV-infected controls. Cells that stained yellow (white arrows) are positive for both GFAP and WNV. The images shown are representative of 3 individual slices.

determined by reduced microtubule-associated protein 2 (MAP2) staining and the presence of shorter neuronal processes (Fig. 3B). Interestingly, costaining of WNV and MAP2 was uncommon and may reflect the lack of MAP2 staining seen in WNV-infected dying neurons. Taken together, these results indicate that inhibition of proinflammatory responses and increased viral load are associated with increased apoptotic neuronal cell death in WNV-infected BSC.

Rosiglitazone enhances the severity of WNV-induced CNS disease in infected mice. Having shown that rosiglitazone decreases WNV-induced neuroinflammation and increases viral load and neuronal death in infected BSC, we wanted to see if rosiglitazone had a similar effect *in vivo*. Swiss Webster mice were fed rosiglitazone chow for 14 days prior to infection with WNV (footpad inoculation, 1,000 PFU). Animals were then monitored daily and were sacrificed when they lost 20% of body weight (a surrogate of fatal disease). Around 50% of rosiglitazone-treated, WNV-infected mice succumbed to WNV infection compared to only 30% of untreated, WNV-infected mice ($P < 0.05$; Fig. 4A). There was no significant change in the day of death for infected mice between treatment groups. All mock-infected mice survived in both treatment groups. Viral titers, determined by plaque assay, were increased in rosiglitazone-treated mice compared to untreated controls at 9 days postinfection (dpi) (Fig. 4B). At 9 dpi, sectioned brains were stained with hematoxylin and eosin (H&E) or incubated with anti-caspase 3, anti-CD3, anti-GFAP, or anti-WNV envelope (WNVE) antibodies. No caspase 3-positive cells and no tissue damage could be seen in sagittal brain sections from any rosiglitazone-treated or untreated mock-infected mice (data not shown). No visible tissue damage was seen in untreated, WNV-infected mice, although occasional caspase 3-positive cells were seen: 1 out of 4 WNV-infected, untreated animals had a total of 5 caspase-positive cells throughout the brain section (Fig. 4C to E). In contrast, although there was a lot of variability in the number of caspase-positive cells in the brains of WNV-infected, rosiglitazone-treated mice, sections from the brains of 4 out of 5 mice contained caspase 3-positive cells, with total numbers ranging from 6 to over

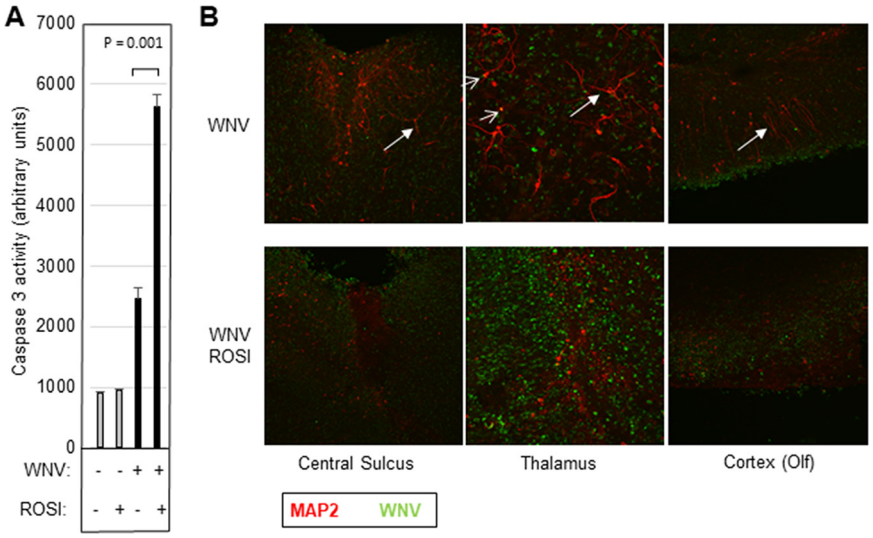

FIG 3 Rosiglitazone treatment increases caspase 3 activity and neuronal death in WNV-infected BSC. BSC were infected with WNV (10^5 PFU per slice) in the presence/absence of 20 μM rosiglitazone (ROSI). Five (caspase 3) or 7 (IHC) days following infection, cultures were harvested for caspase 3 activity assays or were prepared for IHC. (A) *In vitro* caspase 3 activity assays showed that caspase 3 was elevated in WNV-infected BSC compared to uninfected controls and that rosiglitazone treatment augmented WNV-induced caspase 3 activity. The graph shows average caspase 3 activity ($n = 4$). Error bars indicate standard error of the mean. Statistical significance was determined using 2 sample, 2-tailed *t* tests (GraphPad). (B) Immunohistochemistry using antibodies for WNV (green) and the neuronal marker MAP2 (red) demonstrated that titer was increased in rosiglitazone slices and that this was accompanied by increased neuronal death identified by a decrease in MAP2 staining as well as shortening of neuronal processes (white arrows). Neurons costaining with WNV and MAP2 are highlighted (open arrows).

200 (Fig. 4C and D). Tissue damage in rosiglitazone-treated, WNV-infected mice was consistent with caspase staining such that the mouse with the highest number of caspase 3-positive cells demonstrated severe tissue injury and neuronal death characterized by cell body shrinkage and darkly stained pyknotic nuclei that were associated with vacuolation of adjacent tissue (Fig. 4E). Similar to what we observed *in ex vivo* slices, rosiglitazone treatment resulted in higher levels of WNV antigen and GFAP in the brains of WNV-infected mice than untreated controls (Fig. 5A). Although WNV-positive cells were not seen in the brains of untreated, infected mice at 9 days postinfection, increased T cell (CD3) staining in untreated, WNV-infected mice compared to mock-infected controls provided evidence of infection (Fig. 5B and C), consistent with plaque assay data (Fig. 4B). Overall, CD3 staining reflected the extent of tissue damage. with high numbers of lymphocytes present in the most severely damaged brain sections from rosiglitazone-treated, WNV-infected mice.

DISCUSSION

WNV infection of CNS tissue *in vivo* and in *ex vivo* BSC and SCSC results in a robust neuroinflammatory response that includes the increased expression of proinflammatory chemokines and cytokines and activation of astrocytes and microglia (4, 11, 22, 34). *In vivo*, these responses have been shown to influence the infiltration and function of peripheral immune cells, which is critical for viral clearance and protection from CNS disease (14, 17, 19, 24, 25). However, whether these intrinsic neuroinflammatory responses directly affect virus pathogenesis within the CNS and function in the absence of peripheral immune cells is less clear. The PPARγ agonist rosiglitazone inhibits the expression of proinflammatory chemokines and cytokines in the brain and is protective in several models of CNS pathogenesis, including Alzheimer's disease (40), Parkinson's disease (41, 42), amyotrophic lateral sclerosis (43–45), Huntington's disease (43, 46–48), ischemic injury (49), and HIV-associated brain inflammation (39). We used rosiglitazone to investigate the role of neuroinflammation following WNV

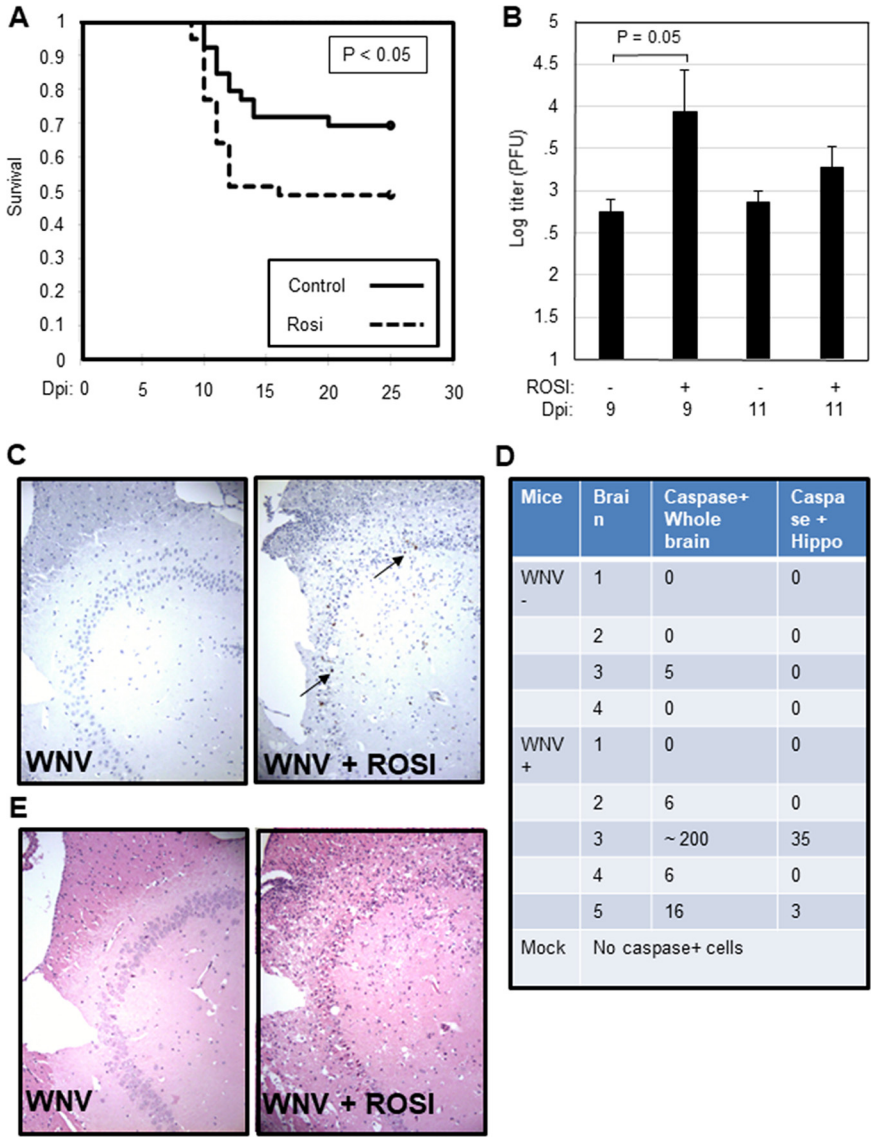

Mice	Brain	Caspase+ Whole brain	Caspase + Hippo
WNV-	1	0	0
	2	0	0
	3	5	0
	4	0	0
WNV+	1	0	0
	2	6	0
	3	~200	35
	4	6	0
	5	16	3
Mock	No caspase+ cells		

FIG 4 Rosiglitazone decreases survival and increases caspase activity and pathology in the brains of WNV-infected mice. Mice were fed rosiglitazone ($n = 20$) or control ($n = 20$) chow for 14 days prior to infection with 1000 PFU WNV (NY99) by footpad inoculation. The displayed data reflects 2 independent experiments (10 mice per condition per experiment). Animals were then monitored daily for weight loss (a surrogate marker for survival). Animals were sacrificed when they had lost 20% of their body weight. (A) Graph shows the percentage of animals that maintained at least 80% of body weight following infection. (B) At 9 and 11 dpi, brains were harvested, and WNV titer was determined by plaque assay. The mean viral titer is shown ($n = 6$ for treated and untreated animals at 9 dpi; $n = 4$ for treated animals at 11 dpi since 2 animals were sacrificed due to unacceptable loss of body weight). Error bars represent SEM. Statistical significance was determined using 2-sample, 2-tailed *t* tests (GraphPad). Brains of rosiglitazone and untreated, mock-infected, and WNV-infected mice were harvested at 9 dpi and were sectioned and stained with antibodies directed against activated caspase 3 ($n = 5$ for mock-infected and treated-infected mice, $n = 4$ for untreated, infected mice). (C) Images show caspase 3 staining in the rosiglitazone-treated, WNV-infected mouse with the most caspase 3-positive cells compared to that seen in an untreated, WNV-infected control. Caspase 3-positive cells are highlighted (arrow). (D) Table shows the number of activated-caspase 3-positive cells in the whole section or localized to the hippocampus in WNV-infected/untreated mice (WNV−, $n = 4$) or WNV-infected/rosiglitazone-treated (WNV+, $n = 5$) mice. No cells containing activated caspase 3 were seen in treated or untreated mock-infected animals. (E) At 9 dpi, H&E-stained sections showed tissue damage in rosiglitazone-treated, WNV-infected mice that was consistent with caspase staining such that the mouse with the highest number of caspase 3-positive cells demonstrated severe tissue injury and neuronal death characterized by cell body shrinkage and darkly staining pyknotic nuclei that were associated with vacuolation of adjacent tissue.

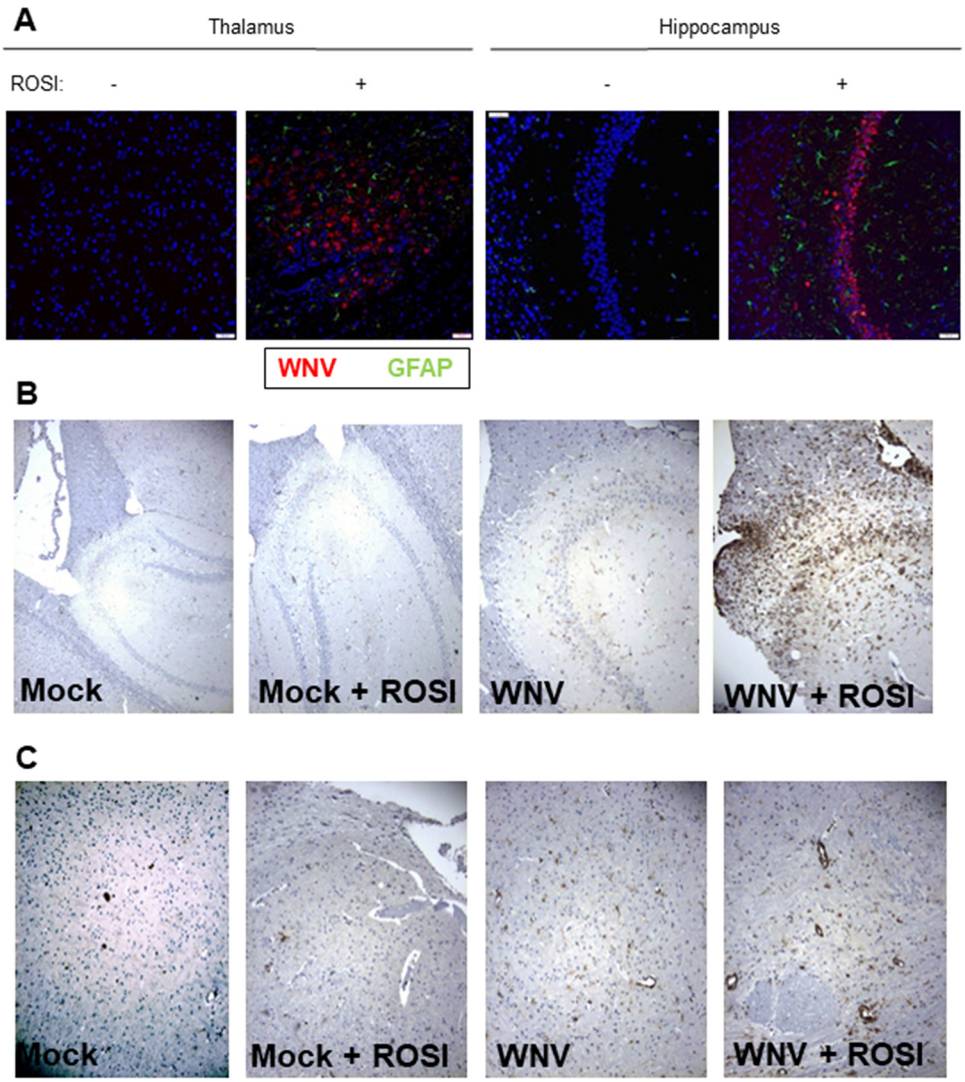

FIG 5 Rosiglitazone increases the activation of astrocytes, viral growth, and lymphocyte infiltration in the brains of WNV-infected mice. Mice were fed rosiglitazone chow for 14 days prior to footpad inoculation of 1000 PFU WNV (NY99). At 9 days postinfection, brains were harvested, sectioned, and stained with antibodies directed against GFAP (A), WNVE (A), or CD3 (B and C). Similar to what we observed in *ex vivo* slices, and consistent with data presented in Fig. 4, rosiglitazone treatment resulted in higher levels of WNV antigen (red staining) (A), GFAP (green staining) (A), and CD3 (B and C) in the thalamus (A), hippocampus (A and B), and cortex (C) of the WNV-infected/rosiglitazone-treated, WNV-infected mouse with the highest caspase 3 positivity and greatest level of injury compared to an untreated, WNV-infected, control. Increased CD3 staining is also seen in the hippocampus (B) and cortex (C) of an untreated, WNV-infected mouse compared to mock-infected controls.

infection of *ex vivo* BSC. BSC are isolated from peripheral immune responses and provide a convenient model system in which intrinsic CNS effects can be investigated in the absence of infiltrating immune cells. As expected (34–39), rosiglitazone treatment resulted in widespread inhibition of WNV-induced expression of proinflammatory chemokines (CXCL10, CCL5, and CCL2) and cytokines (TNF-α and IL-6), which was associated with reduced activation of microglia. However, instead of being protective, as has been shown in other models of CNS injury and disease, rosiglitazone treatment of WNV-infected BSC resulted in increased viral load, caspase 3 activation, and neuronal death. Rosiglitazone had a similar effect *in vivo*, increasing the severity of WNV-induced CNS disease in mice.

It is unlikely that the decreased expression of proinflammatory genes following rosiglitazone treatment of WNV-infected BSC directly contributes to increased viral load and virus-induced neuronal death. Indeed, a reduction in WNV-induced expression of

TNF-α, which is thought to contribute to neuronal death following WNV infection (36, 37), and IL-6 (50) would be expected to promote neuronal survival. However, the reduced activation of microglia, seen following rosiglitazone treatment of WNV-infected BSC, would likely result in increased viral load based on studies which show that pharmacologic deletion of microglia results in increased viral burden in the CNS and higher mortality in infected mice (23, 24). Increased viral load in the absence of microglia *in vivo* has been attributed to the ability of microglia to attract and regulate the function of infiltrating immune cells (24, 51). Our observation that a decrease in microglial activation is associated with increased viral load in WNV-infected BSC now suggests that microglia have additional effects that are intrinsic to the CNS. We have previously shown that microglia phagocytoze WNV-infected cells in BSC (11), providing a mechanism by which a lack of activated microglia would result in increased viral load. Another possible mechanism by which microglia could result in increased viral load is through type 1 IFN signaling. Type 1 IFN signaling is perhaps the most well-characterized innate immune response to viral infection and is critical for limiting viral multiplication (27, 28). Following viral infection, viral sensors, including RigI-like helicases (RLRs), recognize viral pathogen-associated molecular patterns (PAMPS), leading to a signaling cascade mediated by mitochondrial antiviral signaling (MAVS) and resulting in the activation of interferon regulatory factor 3 (IRF3) and NF-κB (52). Simplistically, NF-κB then goes on to regulate the expression of proinflammatory genes, whereas IRF3 promotes the upregulation of type 1 IFNs and the subsequent expression of ISG, which function to inhibit viral multiplication (53). Astrocytes (54) and neurons (55) can release type 1 IFNs following WNV infection; however, microglial release of type 1 IFNs has been shown to be critically important for the control of viral multiplication and injury in the CNS following viral infection (27, 51, 56). Additional work in our laboratory has shown that the expression of IFN-β is not reduced in WNV-infected BSC that are depleted in microglia (S. Stonedahl, personal communication), indicating that microglia are not the primary source of type I IFNs following WNV infection of BSC and suggesting that rosiglitazone interferes with type I IFN production in WNV-infected neurons and astrocytes. Rosiglitazone could also inhibit the expression of IFN-β signaling through its ability to inhibit NF-κB signaling (57), which can result in decreased activation of microglia (58).

Our current observation that decreased microglial activation is associated with increased viral multiplication and virus-induced neuronal death following rosiglitazone treatments appears to contradict our previous studies with minocycline (34). Minocycline is a tetracycline antibiotic that can inhibit the activation of microglia. In WNV-infected SCSC, the inhibition of microglia activation following minocycline treatment was associated with unchanged or slightly reduced viral load and increased neuronal survival (34). It is possible that these differences are due to the different CNS tissue used (BSC compared to SCSC). However, a more likely explanation stems from the fact that minocycline has been shown to directly inhibit WNV replication and WNV-induced apoptosis (59).

In contrast to microglia, astrocyte activation was not inhibited in rosiglitazone-treated, WNV-infected BSC. In fact, rosiglitazone treatment resulted in increased expression of GFAP mRNA and increased numbers of GFAP-positive cells in WNV-infected BSC and brains. Reports in the literature also suggest that rosiglitazone treatment may increase GFAP expression (57, 60). Astrocytes can be activated by UV-inactivated supernatant from WNV-infected neurons (32). Since a higher number of neurons are infected in the presence of rosiglitazone, this could also account for increased GFAP positivity in WNV-infected treated tissue compared to untreated, WNV-infected controls.

MATERIALS AND METHODS

Mice. Eight- to 10-week-old Swiss Webster mice of both sexes were used for this study (Envigo). In our previous studies, we have found no significant difference in lethality between WNV-infected male and female Swiss Webster mice. Mice were observed and weighed daily to monitor disease progression. All experiments were approved by the Institutional Animal Care and Use Committee (IACUC). Where indicated, mice were fed rosiglitazone chow (Research Diets; catalog no. D12492) or a control diet (Research Diets; catalog no. D12450B) starting 14 days prior to infection.

Virus. West Nile virus stocks were obtained from clone-derived strain 385-99 (NY99) as previously described (61). Briefly, virus was propagated in Vero cells following a passage through C6/36 mosquito cells to amplify the virus. Following the observation of cytopathic effect *in vitro*, virus was purified through sucrose cushion ultracentrifugation to remove cellular debris and associated growth factors. Virus stocks were diluted to the indicated inoculum in sterile phosphate-buffered saline and injected in the left rear footpad or were used to infect *ex vivo* brain slice cultures as described below. The titer of virus was determined by PCR (see below) or plaque assay.

Brain slice cultures. BSC were prepared from neonatal (3- to 4-day-old) NIH Swiss Webster mice as we have previously described (4, 11) in compliance with IACUC protocols and institutional guidelines at the University of Colorado, Anschutz Medical Campus. Briefly, brains were removed and embedded in 2% agarose and mounted onto a Vibratome cutting instrument (VT1000S; Leica). Transverse sections (400 μm) were sliced and collected in medium (Dulbecco's modified Eagle's medium; 10 mM Tris, 28 mM D-glucose, pH 7.2). Sections were removed from the agarose and plated onto 30-mm 0.4-μm pore-size cell culture membrane inserts (Millipore), which transferred to 35-mm well plates containing 1.1 ml culture medium (neurobasal A; 10 mM HEPES, 400 μM L-glutamine, 600 μM GlutaMAX, 1 μM B27 [Invitrogen], 60 μg/ml streptomycin, 60 U/ml penicillin, and 6 U/ml nystatin) supplemented with 10% fetal bovine serum (FBS). Slices were maintained at 5% CO_2 in a cell culture incubation chamber. The next day, new culture medium was added with 5% FBS, and 2 days later, the medium was changed without FBS supplementation. Medium changes were then repeated every 2 days. Rosiglitazone (Sigma; catalog no. R2408) and GW9622 (Sigma; catalog no. M6191) were added to media at a final concentration of 20 μM in dimethyl sulfoxide (DMSO). Three days after preparing BSC (when the medium was changed without FBS supplement), BSC were inoculated directly with 1×10^5 PFU/slice in a volume of 20 μl culture medium. BSC were washed 12 h later to remove excess medium and virus.

IHC. Brain tissue was fixed in 10% formalin for 20 h at room temperature. Tissue was transferred into 70% ethanol before paraffin embedding and cutting of sections. Coronal brain sections (4 μm thick) were prepared, and tissue injury was assessed semiquantitatively in H&E-stained tissue. Alternatively, sections were deparaffinized in xylene and rehydrated in consecutive 100% to 75% ethanol washes. Antigen retrieval was performed using antigen-unmasking solution (Vector Laboratories) or 10 mM citrate buffer (pH 6.0). Tissue sections were permeabilized in Neuropore (Trevigen, Gaithersburg, MD) overnight at 4°C and blocked in 10% normal goat serum (NGS) in Tris-buffered saline with Tween 20 (TBST) for 6 to 8 h at room temperature. Sections were then incubated overnight with primary antibodies, including rabbit anti-Iba1 (1:500; Wako), rabbit anti-GFAP (1:900; Abcam), rabbit anti-MAP2 (1:100; Millipore), mouse anti-WNV envelope protein (1:200; ATCC), rabbit anti-active caspase 3 (1:100; Cell Signaling), and CD3 (1:500; Invitrogen). For diaminobenzidine (DAB) staining, sections were washed with TBST before being incubated with biotinylated secondary antibody (Vector Laboratories) diluted in 5% NGS-TBST for 2 h at room temperature. Following further washes in TBST, sections were incubated in 0.6% H_2O_2 (25 min) and ABC reagent (Vector Laboratories) (for 1 h) before incubation for up to 10 min in prewarmed DAB (Trevigen, Gaithersburg, MD). Blue counterstain (Trevigen) was applied to sections before dehydrating and mounting with VectaMount (Vector Laboratories). For fluorescent colabeling studies, following binding of primary antibody, sections were washed and incubated with secondary antibodies (goat anti-mouse Alexa Fluor 568 and goat anti-rabbit Alexa Fluor 488; 1:1,000; Invitrogen). Coverslips were applied using ProLong Gold antifade reagent (Molecular Probes). BSC were washed in phosphate-buffered saline (PBS) and fixed in 10% neutral buffered formalin for at least 1 h. The fixed BSC were rewashed in PBS, immersed in block solution (PBS, 4% normal goat serum, 2% bovine serum albumin, and 0.3% Triton X) for 1 h, and then incubated overnight at room temperature with primary antibodies (see above) diluted in block solution. The next day, the BSC were washed 3 times with wash solution (PBS, 0.3% Triton X) and then incubated for 2 h at room temperature with secondary antibodies (see above) in block solution. After being washed 3 more times with wash solution, the BSC were briefly rinsed with distilled water (dH_2O) before being mounted onto microscopy slides with ProLong Gold antifade reagent (Molecular Probes). All slides (brain sections and BSC) were imaged using a Zeiss Axiocam on a Nikon Eclipse E800 epifluorescence microscope, with image procurement conducted with AxioVision software (v4.8; Zeiss).

RT-qPCR. BSC were removed from filters and homogenized in RLT buffer (Qiagen) with 1% beta-mercaptoethanol and loaded onto RNeasy spin columns (Qiagen), and purified RNA was collected following the manufacturer's protocols for the RNeasy minikit (Qiagen). The RNA quality and concentration were measured with an Agilent 2100 bioanalyzer, and cDNA was prepared with iScript (Bio-Rad) following the manufacturer's directions. For determination of cellular gene expression, the cDNA was mixed with appropriate primers (Bio-Rad) and 2 μl SYBR green master mix (SA Biosciences) to 20-μl volumes in individual wells of a 96-well PCR plate, and PCR amplification was performed with a CFX96 thermocycler (Bio-Rad). Relative gene expression was determined via threshold cycle analysis using Bio-Rad CFX Manager software. Beta-actin expression was the control gene setting, and untreated, mock-infected BSC was the normalization set point for individual gene analyses. For determination of viral titer, equivalent volumes of cDNA were used for PCR with degenerate primers targeting the VP1 gene (PCR protocol, 95°C 3 min, 40× cycles of 95°C for 10 s, 53°C for 30 s, and 72°C for 30 s; melt curves, 65 to 95°C in 0.5°C steps). Samples were compared to a plasmid standard curve. Temperature melt curves temperature and slope were used to assess the quality of each sample. The starting genome copy number for each dilution of the standard curve was estimated using spectrophotometer data. The starting genome copy number per microliter was correlated with the resulting cycle threshold (C_T) value at each dilution in the standard curve, and the standard curve equation was calculated using Excel (Microsoft, Redmond, WA).

ELISA. BSC were collected in lysis buffer (R&D) and homogenized/sonicated to create lysate to screen with a custom Mouse Mix & Match Cytokine ELISArray strip kit (Signosis). Lysate was added to ELISArray plate wells for 2 h of binding incubation, and the plates were washed 3 times and then incubated for 1 h with streptavidin-bound detection antibody. After 3 additional washes, streptavidin horseradish peroxidase (HRP) solution was incubated for 45 min. Detection solution was then added to each well for 30 min before stop solution was applied, turning the solution yellow, depending on the amount of bound detection antibody. The strength of the yellow color was quantified colorimetrically at 450 nm with an EMax spectrometer (Molecular Devices).

Statistical analysis. All PCR and ELISA graphs, Kaplan Meier survival curves, and statistical analysis were created and assessed with GraphPad InStat and Prism software. Two-sample, 2-tailed *t* tests will be used to compare data from treated and untreated conditions at individual time points. Survival analysis will be conducted using Kaplan-Meier plots, and heterogeneity between the treatment groups will be tested with the log-rank (Mantel-Cox) test.

ACKNOWLEDGMENTS

This work was supported by the Department of Veteran's Affairs (merit award BX000963) and the National Institutes of Health (R01 NS076512).

K.L.T. is the Louise Baum Endowed Professor and Chair.

REFERENCES

1. Kramer LD, Li J, Shi PY. 2007. West Nile virus. Lancet Neurol 6:171–181. https://doi.org/10.1016/S1474-4422(07)70030-3.
2. Bode AV, Sejvar JJ, Pape WJ, Campbell GL, Marfin AA. 2006. West Nile virus disease: a descriptive study of 228 patients hospitalized in a 4-county region of Colorado in 2003. Clin Infect Dis 42:1234–1240. https://doi.org/10.1086/503038.
3. Winkelmann ER, Luo H, Wang T. 2016. West Nile virus infection in the central nervous system. F1000Res 5:105. https://doi.org/10.12688/f1000research.7404.1.
4. Clarke P, Leser JS, Quick ED, Dionne KR, Beckham JD, Tyler KL. 2014. Death receptor-mediated apoptotic signaling is activated in the brain following infection with West Nile virus in the absence of a peripheral immune response. J Virol 88:1080–1089. https://doi.org/10.1128/JVI.02944-13.
5. Samuel MA, Morrey JD, Diamond MS. 2007. Caspase 3-dependent cell death of neurons contributes to the pathogenesis of West Nile virus encephalitis. J Virol 81:2614–2623. https://doi.org/10.1128/JVI.02311-06.
6. Fratkin JD, Leis AA, Stokic DS, Slavinski SA, Geiss RW. 2004. Spinal cord neuropathology in human West Nile virus infection. Arch Pathol Lab Med 128:533–537. https://doi.org/10.5858/2004-128-533-SCNIHW.
7. Hayes EB, Sejvar JJ, Zaki SR, Lanciotti R, Bode AV, Campbell GL. 2005. Virology, pathology, and clinical manifestations of West Nile virus disease. Emerg Infect Dis 11:1174–1179. https://doi.org/10.3201/eid1108.050289b.
8. Szretter KJ, Samuel MA, Gilfillan S, Fuchs A, Colonna M, Diamond MS. 2009. The immune adaptor molecule SARM modulates tumor necrosis factor alpha production and microglia activation in the brainstem and restricts West Nile virus pathogenesis. J Virol 83:9329–9338. https://doi.org/10.1128/JVI.00836-09.
9. Sabouri AH, Marcondes MCG, Flynn C, Berger M, Xiao N, Fox HS, Sarvetnick NE. 2014. TLR signaling controls lethal encephalitis in WNV-infected brain. Brain Res 1574:84–95. https://doi.org/10.1016/j.brainres.2014.05.049.
10. Vidaña B, Johnson N, Fooks AR, Sánchez-Cordón PJ, Hicks DJ, Nuñez A. 2020. West Nile virus spread and differential chemokine response in the central nervous system of mice: role in pathogenic mechanisms of encephalitis. Transbound Emerg Dis 67:799–810. https://doi.org/10.1111/tbed.13401.
11. Quick ED, Leser JS, Clarke P, Tyler KL. 2014. Activation of intrinsic immune responses and microglial phagocytosis in an ex vivo spinal cord slice culture model of West Nile virus infection. J Virol 88:13005–13014. https://doi.org/10.1128/JVI.01994-14.
12. van Marle G, Antony J, Ostermann H, Dunham C, Hunt T, Halliday W, Maingat F, Urbanowski MD, Hobman T, Peeling J, Power C. 2007. West Nile virus-induced neuroinflammation: glial infection and capsid protein-mediated neurovirulence. J Virol 81:10933–10949. https://doi.org/10.1128/JVI.02422-06.
13. Daniels BP, Jujjavarapu H, Durrant DM, Williams JL, Green RR, White JP, Lazear HM, Gale M, Diamond MS, Klein RS. 2017. Regional astrocyte IFN signaling restricts pathogenesis during neurotropic viral infection. J Clin Invest 127:843–856. https://doi.org/10.1172/JCI88720.
14. Klein RS, Lin E, Zhang B, Luster AD, Tollett J, Samuel MA, Engle M, Diamond MS. 2005. Neuronal CXCL10 directs CD8+ T-cell recruitment and control of West Nile virus encephalitis. J Virol 79:11457–11466. https://doi.org/10.1128/JVI.79.17.11457-11466.2005.
15. Sitati EM, Diamond MS. 2006. CD4+ T-cell responses are required for clearance of West Nile virus from the central nervous system. J Virol 80:12060–12069. https://doi.org/10.1128/JVI.01650-06.
16. Zhang B, Chan YK, Lu B, Diamond MS, Klein RS. 2008. CXCR3 mediates region-specific antiviral T cell trafficking within the central nervous system during West Nile virus encephalitis. J Immunol 180:2641–2649. https://doi.org/10.4049/jimmunol.180.4.2641.
17. Glass WG, Lim JK, Cholera R, Pletnev AG, Gao JL, Murphy PM. 2005. Chemokine receptor CCR5 promotes leukocyte trafficking to the brain and survival in West Nile virus infection. J Exp Med 202:1087–1098. https://doi.org/10.1084/jem.20042530.
18. Bréhin AC, Mouriès J, Frenkiel MP, Dadaglio G, Despres P, Lafon M, Couderc T. 2008. Dynamics of immune cell recruitment during West Nile encephalitis and identification of a new CD19+B220-BST-2+ leukocyte population. J Immunol 180:6760–6767. https://doi.org/10.4049/jimmunol.180.10.6760.
19. Lim JK, Obara CJ, Rivollier A, Pletnev AG, Kelsall BL, Murphy PM. 2011. Chemokine receptor Ccr2 is critical for monocyte accumulation and survival in West Nile virus encephalitis. J Immunol 186:471–478. https://doi.org/10.4049/jimmunol.1003003.
20. Sitati E, McCandless EE, Klein RS, Diamond MS. 2007. CD40-CD40 ligand interactions promote trafficking of CD8+ T cells into the brain and protection against West Nile virus encephalitis. J Virol 81:9801–9811. https://doi.org/10.1128/JVI.00941-07.
21. Getts DR, Terry RL, Getts MT, Muller M, Rana S, Shrestha B, Radford J, Van Rooijen N, Campbell IL, King NJC. 2008. Ly6c+ "inflammatory monocytes" are microglial precursors recruited in a pathogenic manner in West Nile virus encephalitis. J Exp Med 205:2319–2337. https://doi.org/10.1084/jem.20080421.
22. Clarke P, Leser JS, Bowen RA, Tyler KL. 2014. Virus-induced transcriptional changes in the brain include the differential expression of genes associated with interferon, apoptosis, interleukin 17 receptor A, and glutamate signaling as well as flavivirus-specific upregulation of tRNA synthetases. mBio 5:e00902-14. https://doi.org/10.1128/mBio.00902-14.
23. Seitz S, Clarke P, Tyler KL. 2018. Pharmacologic depletion of microglia increases viral load in the brain and enhances mortality in murine models of flavivirus-induced encephalitis. J Virol 92:e00525-18. https://doi.org/10.1128/JVI.00525-18.
24. Funk KE, Klein RS. 2019. CSF1R antagonism limits local restimulation of antiviral CD8+ T cells during viral encephalitis. J Neuroinflammation 16:22. https://doi.org/10.1186/s12974-019-1397-4.
25. Shrestha B, Zhang B, Purtha WE, Klein RS, Diamond MS. 2008. Tumor necrosis factor alpha protects against lethal West Nile virus infection by promoting trafficking of mononuclear leukocytes into the central nervous system. J Virol 82:8956–8964. https://doi.org/10.1128/JVI.01118-08.
26. Velazquez-Salinas L, Verdugo-Rodriguez A, Rodriguez LL, Borca MV. 2019. The role of interleukin 6 during viral infections. Front Microbiol 10:1057. https://doi.org/10.3389/fmicb.2019.01057.

27. Drokhlyansky E, Goz Ayturk D, Soh TK, Chrenek R, O'Loughlin E, Madore C, Butovsky O, Cepko CL. 2017. The brain parenchyma has a type I interferon response that can limit virus spread. Proc Natl Acad Sci U S A 114:E95–E104. https://doi.org/10.1073/pnas.1618157114.
28. Hwang M, Bergmann CC. 2019. Intercellular communication is key for protective IFN alpha/beta signaling during viral central nervous system infection. Viral Immunol 32:1–6. https://doi.org/10.1089/vim.2018.0101.
29. Stoll G, Jander S, Schroeter M. 2000. Cytokines in CNS disorders: neurotoxicity versus neuroprotection. J Neural Transm Suppl 59:81–89. https://doi.org/10.1007/978-3-7091-6781-6_11.
30. Vasek MJ, Garber C, Dorsey D, Durrant DM, Bollman B, Soung A, Yu J, Perez-Torres C, Frouin A, Wilton DK, Funk K, DeMasters BK, Jiang X, Bowen JR, Mennerick S, Robinson JK, Garbow JR, Tyler KL, Suthar MS, Schmidt RE, Stevens B, Klein RS. 2016. A complement-microglial axis drives synapse loss during virus-induced memory impairment. Nature 534:538–543. https://doi.org/10.1038/nature18283.
31. Leis AA, Grill MF, Goodman BP, Sadiq SB, Sinclair DJ, Vig PJS, Bai F. 2020. Tumor necrosis factor-alpha signaling may contribute to chronic West Nile virus post-infectious proinflammatory state. Front Med 7:164. https://doi.org/10.3389/fmed.2020.00164.
32. Kumar M, Verma S, Nerurkar VR. 2010. Pro-inflammatory cytokines derived from West Nile virus (WNV)-infected SK-N-SH cells mediate neuroinflammatory markers and neuronal death. J Neuroinflammation 7:73. https://doi.org/10.1186/1742-2094-7-73.
33. Quick ED, Seitz S, Clarke P, Tyler KL. 2017. Minocycline has anti-inflammatory effects and reduces cytotoxicity in an *ex vivo* spinal cord slice culture model of West Nile virus infection. J Virol 91:e00569-17. https://doi.org/10.1128/JVI.00569-17.
34. Kapadia R, Yi JH, Vemuganti R. 2008. Mechanisms of anti-inflammatory and neuroprotective actions of PPAR-gamma agonists. Front Biosci 13:1813–1826. https://doi.org/10.2741/2802.
35. Bernardo A, Minghetti L. 2008. Regulation of glial cell functions by PPAR-gamma natural and synthetic agonists. PPAR Res 2008:864140. https://doi.org/10.1155/2008/864140.
36. Yang S, Wang H, Yang Y, Wang R, Wang Y, Wu C, Du G, Xiang B, Xiao C, Shen T, Li XF. 2019. Baicalein administered in the subacute phase ameliorates ischemia-reperfusion-induced brain injury by reducing neuroinflammation and neuronal damage. Biomed Pharmacother 117:109102. https://doi.org/10.1016/j.biopha.2019.109102.
37. Xiang B, Xiao C, Shen T, Li X. 2018. Anti-inflammatory effects of anisalcohol on lipopolysaccharide-stimulated BV2 microglia via selective modulation of microglia polarization and down-regulation of NF-kappaB p65 and JNK activation. Mol Immunol 95:39–46. https://doi.org/10.1016/j.molimm.2018.01.011.
38. Cai W, Yang T, Liu H, Han L, Zhang K, Hu X, Zhang X, Yin K-J, Gao Y, Bennett MVL, Leak RK, Chen J. 2018. Peroxisome proliferator-activated receptor γ (PPARγ): a master gatekeeper in CNS injury and repair. Prog Neurobiol 163–164:27–58. https://doi.org/10.1016/j.pneurobio.2017.10.002.
39. Omeragic A, Hoque MT, Choi UY, Bendayan R. 2017. Peroxisome proliferator-activated receptor-gamma: potential molecular therapeutic target for HIV-1-associated brain inflammation. J Neuroinflammation 14:183. https://doi.org/10.1186/s12974-017-0957-8.
40. Watson GS, Cholerton BA, Reger MA, Baker LD, Plymate SR, Asthana S, Fishel MA, Kulstad JJ, Green PS, Cook DG, Kahn SE, Keeling ML, Craft S. 2005. Preserved cognition in patients with early Alzheimer disease and amnestic mild cognitive impairment during treatment with rosiglitazone: a preliminary study. Am J Geriatr Psychiatry 13:950–958. https://doi.org/10.1176/appi.ajgp.13.11.950.
41. Randy LH, Guoying B. 2007. Agonism of peroxisome proliferator receptor-gamma may have therapeutic potential for neuroinflammation and Parkinson's disease. Curr Neuropharmacol 5:35–46. https://doi.org/10.2174/157015907780077123.
42. Schintu N, Frau L, Ibba M, Caboni P, Garau A, Carboni E, Carta AR. 2009. PPAR-gamma-mediated neuroprotection in a chronic mouse model of Parkinson's disease. Eur J Neurosci 29:954–963. https://doi.org/10.1111/j.1460-9568.2009.06657.x.
43. Kiaei M. 2008. Peroxisome proliferator-activated receptor-gamma in amyotrophic lateral sclerosis and Huntington's disease. PPAR Res 2008:418765. https://doi.org/10.1155/2008/418765.
44. Kiaei M, Kipiani K, Chen J, Calingasan NY, Beal MF. 2005. Peroxisome proliferator-activated receptor-gamma agonist extends survival in transgenic mouse model of amyotrophic lateral sclerosis. Exp Neurol 191:331–336. https://doi.org/10.1016/j.expneurol.2004.10.007.
45. Schütz B, Reimann J, Dumitrescu-Ozimek L, Kappes-Horn K, Landreth GE, Schürmann B, Zimmer A, Heneka MT. 2005. The oral antidiabetic pioglitazone protects from neurodegeneration and amyotrophic lateral sclerosis-like symptoms in superoxide dismutase-G93A transgenic mice. J Neuroscience 25:7805–7812. https://doi.org/10.1523/JNEUROSCI.2038-05.2005.
46. Napolitano M, Costa L, Palermo R, Giovenco A, Vacca A, Gulino A. 2011. Protective effect of pioglitazone, a PPARγ ligand, in a 3 nitropropionic acid model of Huntington's disease. Brain Res Bull 85:231–237. https://doi.org/10.1016/j.brainresbull.2011.03.011.
47. Johri A, Calingasan NY, Hennessey TM, Sharma A, Yang L, Wille E, Chandra A, Beal MF. 2012. Pharmacologic activation of mitochondrial biogenesis exerts widespread beneficial effects in a transgenic mouse model of Huntington's disease. Hum Mol Genet 21:1124–1137. https://doi.org/10.1093/hmg/ddr541.
48. Jin J, Albertz J, Guo Z, Peng Q, Rudow G, Troncoso JC, Ross CA, Duan W. 2013. Neuroprotective effects of PPAR-γ agonist rosiglitazone in N171-82Q mouse model of Huntington's disease. J Neurochem 125:410–419. https://doi.org/10.1111/jnc.12190.
49. Luo Y, Yin W, Signore AP, Zhang F, Hong Z, Wang S, Graham SH, Chen J. 2006. Neuroprotection against focal ischemic brain injury by the peroxisome proliferator-activated receptor-γ agonist rosiglitazone. J Neurochem 97:435–448. https://doi.org/10.1111/j.1471-4159.2006.03758.x.
50. Rothaug M, Becker-Pauly C, Rose-John S. 2016. The role of interleukin-6 signaling in nervous tissue. Biochim Biophys Acta 1863:1218–1227. https://doi.org/10.1016/j.bbamcr.2016.03.018.
51. Wheeler DL, Sariol A, Meyerholz DK, Perlman S. 2018. Microglia are required for protection against lethal coronavirus encephalitis in mice. J Clin Invest 128:931–943. https://doi.org/10.1172/JCI97229.
52. Seth RB, Sun L, Ea CK, Chen ZJ. 2005. Identification and characterization of MAVS, a mitochondrial antiviral signaling protein that activates NF-κB and IRF3. Cell 122:669–682. https://doi.org/10.1016/j.cell.2005.08.012.
53. Pfeffer LM. 2011. The role of nuclear factor κB in the interferon response. J Interferon Cytokine Res 31:553–559. https://doi.org/10.1089/jir.2011.0028.
54. Lindqvist R, Mundt F, Gilthorpe JD, Wölfel S, Gekara NO, Kröger A, Överby AK. 2016. Fast type I interferon response protects astrocytes from flavivirus infection and virus-induced cytopathic effects. J Neuroinflammation 13:277. https://doi.org/10.1186/s12974-016-0748-7.
55. Daffis S, Samuel MA, Keller BC, Gale M, Diamond MS. 2007. Cell-specific IRF-3 responses protect against West Nile virus infection by interferon-dependent and -independent mechanisms. PLoS Pathog 3:e106. https://doi.org/10.1371/journal.ppat.0030106.
56. Nayak D, Johnson KR, Heydari S, Roth TL, Zinselmeyer BH, McGavern DB. 2013. Type I interferon programs innate myeloid dynamics and gene expression in the virally infected nervous system. PLoS Pathog 9:e1003395. https://doi.org/10.1371/journal.ppat.1003395.
57. Kushwaha R, Mishra J, Gupta AP, Gupta K, Vishwakarma J, Chattopadhyay N, Gayen JR, Kamthan M, Bandyopadhyay S. 2019. Rosiglitazone up-regulates glial fibrillary acidic protein via HB-EGF secreted from astrocytes and neurons through PPARγ pathway and reduces apoptosis in high-fat diet-fed mice. J Neurochem 149:679–698. https://doi.org/10.1111/jnc.14610.
58. Santa-Cecília FV, Socias B, Ouidja MO, Sepulveda-Diaz JE, Acuña L, Silva RL, Michel PP, Del-Bel E, Cunha TM, Raisman-Vozari R. 2016. Doxycycline suppresses microglial activation by inhibiting the p38 MAPK and NF-kB signaling pathways. Neurotox Res 29:447–459. https://doi.org/10.1007/s12640-015-9592-2.
59. Michaelis M, Kleinschmidt MC, Doerr HW, Cinatl J. 2007. Minocycline inhibits West Nile virus replication and apoptosis in human neuronal cells. J Antimicrob Chemother 60:981–986. https://doi.org/10.1093/jac/dkm307.
60. Li Y, Yu G, Liu L, Long J, Su S, Zhao T, Liu W, Shen S, Niu X. 2019. Rosiglitazone attenuates cell apoptosis through antioxidative and anti-apoptotic pathways in the hippocampi of spontaneously hypertensive rats. Int J Mol Med 43:693–700. https://doi.org/10.3892/ijmm.2018.3991.
61. Beatman E, Oyer R, Shives KD, Hedman K, Brault AC, Tyler KL, Beckham JD. 2012. West Nile virus growth is independent of autophagy activation. Virology 433:262–272. https://doi.org/10.1016/j.virol.2012.08.016.